



Short communication

Novel bisubstrate uridine-peptide analogues bearing a pyrophosphate bioisostere as inhibitors of human O-GlcNAc transferase

Philip Ryan^{a,b,c}, Yun Shi^d, Mark von Itzstein^d, Santosh Rudrawar^{a,b,c,*}^a Menzies Health Institute Queensland, Griffith University, Gold Coast, QLD 4222, Australia^b School of Pharmacy and Pharmacology, Griffith University, Gold Coast, QLD 4222, Australia^c School of Chemistry, The University of Sydney, NSW 2006, Australia^d Institute for Glycomics, Griffith University, Gold Coast, QLD 4222, Australia

ARTICLE INFO

Keywords:

OGT inhibitor

Pyrophosphate bioisostere

Bisubstrate analogue as inhibitor

O-GlcNAc transferase (OGT)

ABSTRACT

Protein O-linked β -D-N-acetylglucosamine (O-GlcNAc) modification (O-GlcNAcylation), an essential post-translational as well as cotranslational modification, is the attachment of β -D-N-acetylglucosamine to serine and threonine residues of nucleocytoplasmic proteins. An aberrant O-GlcNAc profile on certain proteins has been implicated in metabolic diseases such as diabetes and cancer. Inhibitors of O-GlcNAc transferase (OGT) are valuable tools to study the cell biology of protein O-GlcNAc modification. In this study we report novel uridine-peptide conjugate molecules composed of an acceptor peptide covalently linked to a catalytically inactive donor substrate analogue that bears a pyrophosphate bioisostere and explore their inhibitory activities against OGT by a radioactive hOGT assay. Further, we investigate the structural basis of their activities *via* molecular modelling, explaining their lack of potency towards OGT inhibition.

1. Introduction

The ubiquitously expressed O-GlcNAc transferase (OGT) enzyme boasts numerous vital cellular roles within eukaryotes. It is solely responsible for transferring O-linked N-acetylglucosamine (O-GlcNAc) onto the serine and threonine residues of acceptor substrate proteins (Fig. 1). OGT employs the universal donor substrate sugar nucleotide (UDP-GlcNAc) to modify myriads of proteins, modulating their functions, processing and associated signalling pathways [1]. Indeed, more than 4000 proteins have been identified as O-GlcNAcylation (O-GlcNAc modification) candidates. O-GlcNAcylation roles are numerous and range from coupling metabolic status to the regulation of an extensive variety of cellular signalling pathways [2–5]. Understandably, dysregulation of protein O-GlcNAcylation is linked to the pathological progression of various chronic metabolic diseases including diabetes [6,7], cancers [8–10] to cardiovascular [11] and neurodegenerative disorders [12–14]. The consequences of cellular hyper-O-GlcNAcylation, *via* both knockout and chemical inhibition of O-GlcNAc hydrolase (OGA) [15], the counterpart O-GlcNAc cleavage enzyme, have been extensively studied [12,16]. The investigation of the precise biological functions as well as implications of cellular hypo-O-GlcNAcylation *via* OGT inhibition has been significantly impeded due to a marked lack of OGT

inhibitors [17].

UDP, the by-product of O-GlcNAcylation, is a potent feedback inhibitor of OGT and has been observed to occupy the same UDP-GlcNAc binding pocket in OGT competitively [18]. Many of the more potent OGT inhibitors have been designed to engage the UDP binding site where they exploit the native binding mode of the donor substrate UDP-GlcNAc [19,20]. The most widely employed inhibitor to date, per-O-acetylated 5-thio-N-acetylglucosamine, hijacks the hexosamine biosynthetic pathway (HBP) to yield the donor substrate analogue UDP-5S-GlcNAc [21]. As UDP is commonly employed as donor substrate by other enzymes, including oxidoreductases, transferases, hydrolases, lyases and isomerases, UDP analogues suffer limited selectivity for OGT.

The structure of ternary hOGT complexes (OGT-UDP-substrate peptide derived from the casein kinase II) have revealed that glycosyltransferase takes place via an ordered bi-bi kinetic mechanism, wherein UDP-GlcNAc binds prior to the polypeptide substrate [18]. The way in which OGT targets specific sites on a limited subset of intracellular proteins remains largely unknown however. Furthermore, the involvement of a catalytic base in the OGT-catalysed glycosyl transfer reaction is currently debated [22–24] and the precise catalytic mechanism of OGT remains to be discovered. As a member of Glycosyltransferase Family 41 (GT41), OGT possesses a GT-B fold and the glycosyl transfer

* Corresponding author.

E-mail address: s.rudrawar@griffith.edu.au (S. Rudrawar).<https://doi.org/10.1016/j.bioorg.2021.104738>

Received 12 September 2020; Received in revised form 4 February 2021; Accepted 5 February 2021

Available online 13 February 2021

0045-2068/© 2021 Elsevier Inc. All rights reserved.

reaction proceeds with inversion of stereochemistry at the anomeric center. Bisubstrate mimics of the transition state structure have emerged as promising, selective inhibitors. These compounds are designed to couple the high affinity of the donor substrate and high selectivity of the acceptor substrate (Fig. 1). Bisubstrate analogue antagonists that are constructed from covalently-linked bridging donor and acceptor substrates, may allow each substrate to occupy their natural orientations within their respective binding sites, affecting the antagonists potency [25].

A number of bisubstrate analogue inhibitors of OGT have been reported. Goblin1 is a UDP-peptide conjugate bearing sequence VTPVS(O-propyl-UDP)_{TA} tethered via an ether linkage [26]. Goblin1 was found to inhibit glycosylation of an acceptor substrate *in vitro* in a dose-dependent manner ($IC_{50} = 18 \mu\text{M}$). Goblin1 was unable to efficiently penetrate cells however, likely as it possessed pyrophosphate in its structure. A second series of bisubstrate analogue inhibitors, bearing neutral aliphatic linker units in place of the natural substrate's pyrophosphate moiety, produced only modest inhibitors of OGT activity [27]. Finally, van Aalten and co-workers produced bisubstrate inhibitors such as the thiol-linked VPTVC(S-propyl-UDP)_{TA} conjugate, functionalised with cell-penetrant peptide sequences, specifically Penetratin and TAT [28,29], to promote cellular uptake [30]. The Goblin bisubstrate cell penetrating conjugate displayed hOGT inhibition ($IC_{50} = 5 \mu\text{M}$) *in vitro* as a parent compound, however conjugates could not target cytosolic hOGT due to entrapment in the early endosomes [30].

Pyrophosphate units tends to confer an increase in potency and a decrease in cell-permeability when implemented into the bisubstrate scaffold. Use of a pyridine unit as a pyrophosphate surrogate has provided compounds with moderate *in vitro* inhibition hOGT [31]. High-throughput screens have found that compounds mimicking pyrophosphate exhibit exquisite inhibition of OGT [32,33]. A series of compounds bearing a five heteroatom dicarbamate core were found to occupy pyrophosphate's position within the OGT enzyme's catalytic site. Investigation into the mechanism of OGT inhibition suggested that the dicarbamate scaffold maintains the potential to deactivate a wide assortment of enzymes that also utilise pyrophosphate-based substrates. Pyrophosphate groups augment potential substrates with limited bioavailability, physiological instability, inability to permeate membranes and also complicate synthetic methods. We were interested to explore if employing a bioisosteric replacement for the pyrophosphate moiety in the design of novel bisubstrate inhibitors of OGT would bypass these issues and afford potency. The diketocyclobutane diamine, or 'squaramide', function has become a well-established phosphate bioisostere owing to its remarkable chemical stability, hydrogen-bonding capability and high double acidity with its resonance-stabilised dianion (Fig. 2a) [34]. Secondary squaramides offer the potential to hydrogen-bond to acceptors, donors and mixed acceptor-donor groups, strengthened by an increase in their aromaticity on complexing [35,36]. Indeed, squaramides have been used to replace phosphate as internucleotidic linkers in the structures of sugar-nucleotide analogues

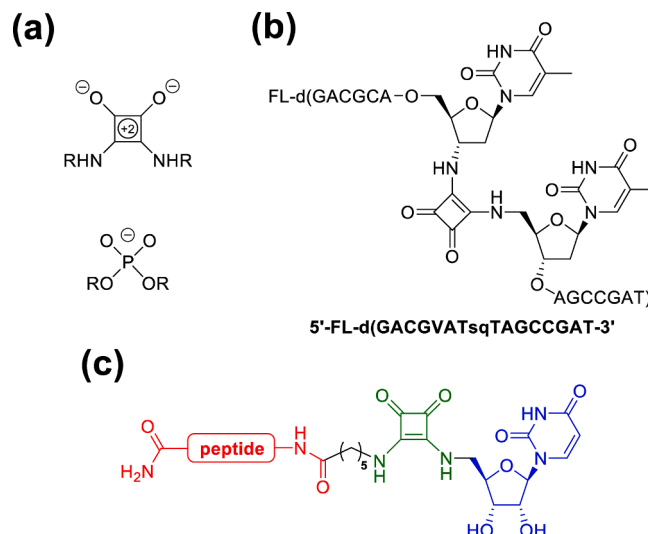


Fig. 2. (a) The structures of the squaramide and phosphate functional groups; (b) An expanded region of a modified oligodeoxynucleotide. The central thymidine dimer has been modified with a squaryldiamide linkage (TsqT). (c) The generalised structure for the squaramide-linked bisubstrate analogue OGT inhibitors described here.

suggested for use as antiviral and anticancer agents (Fig. 2b) [37,38]. The inhibitors here employ the squaramide bioisostere to exploit pyrophosphate's role in establishing stabilising interactions during the transfer reaction within the active site of OGT (Fig. 2c). Here we disclose the rational design, synthesis and evaluation of some novel bisubstrate analogue inhibitors against the hOGT enzyme (Fig. 3).

2. Materials and methods

2.1. General

^1H NMR spectra were recorded using Bruker Avance 300, Avance III 400 and Avance III 500 spectrometers at frequencies of 300 MHz, 400 MHz and 500 MHz respectively. The spectra are reported as parts per million (ppm) downfield shift using the solvent peak as internal reference. The data are reported as chemical shift (δ), multiplicity, relative integral, coupling constant (J Hz) and assignment where possible. Low resolution mass spectra were recorded on a Finnigan LCQ Deca ion trap mass spectrometer (ESI). High resolution mass spectra were recorded on a Bruker 7 T Fourier Transform Ion Cyclotron Resonance Mass Spectrometer (FTICR). Analytical reverse-phase HPLC was performed on a Shimadzu LCMS 2020 separations module with an LC-20AD pump and SPD-20A photodiode array detector. A Waters Sunfire C18 $5 \mu\text{m}$, $2.1 \times 150 \text{ mm}$ column was used at a flow rate of 0.2 mL min^{-1} using a mobile

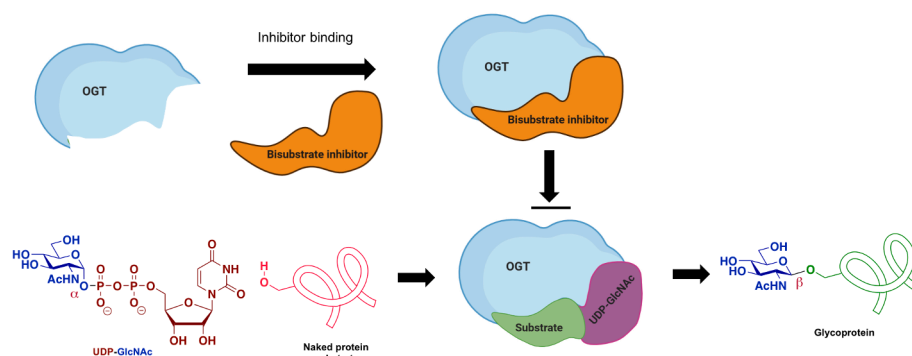


Fig. 1. OGT catalysed O-GlcNAcylation and bisubstrate analogue as OGT inhibitor.

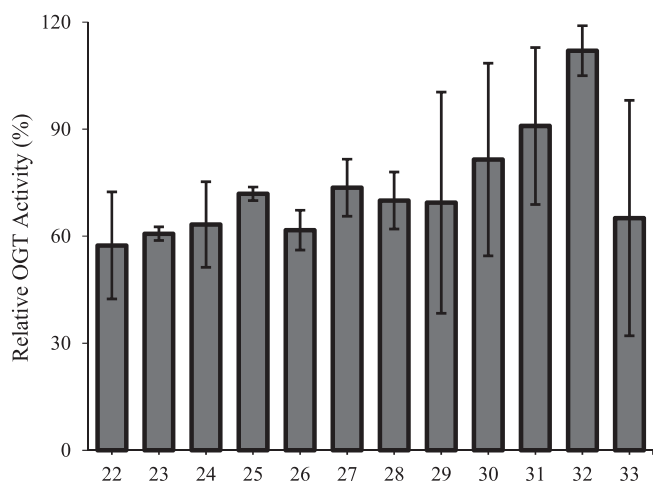


Fig. 3. Antagonistic activity was evaluated by a radioactive hOGT assay using recombinant nup62-MBP fusion construct as the protein acceptor and [^3H]-UDP-GlcNAc in UDP-GlcNAc as competitive donor substrate. Reactions were performed in duplicate with inhibition measured as a percentage of relative OGT activity in absence of inhibitor. All compounds assayed at 20 μM concentration.

phase of 0.1% TFA in water (Solvent A) and 0.1% TFA in acetonitrile (Solvent B) and a linear gradient of 2–50% B over 30 min. The results were analysed with Waters Empower software. Preparative reverse-phase HPLC was performed using a Waters 600 Multisolvant Delivery System and Waters 500 pump with 2996 photodiode array detector or Waters 490E Programmable wavelength detector operating at 214 and 254 nm. A Waters Sunfire 5 μm , 19 \times 150 mm column was used at a flow rate of 7 mL min^{-1} using a mobile phase of 0.1% TFA in water (Solvent A) and 0.1% TFA in acetonitrile (Solvent B) using a linear gradient of one of either i) 2–80% B over 60 min, ii) 2–60% B over 60 min or 2–40% over 60 min. LC-MS was performed on a Shimadzu LCMS 2020 system coupled with an LC-20AD pump and SPD-20A detector on a Waters Sunfire C18 5 μm , 2.1 \times 150 mm column at a flow rate of 0.2 mL min^{-1} coupled to a Thermoquest Finnigan LCQ Deca mass spectrometer (ESI) operating in positive mode. Separations involved a mobile phase of 0.1% formic acid in water (Solvent A) and 0.1% formic acid in acetonitrile (Solvent B) using a linear gradient of 2–50% B over 30 min. Analytical thin layer chromatography (TLC) was performed on commercially prepared silica plates (Merck Kieselgel 60 0.25 mm F254). Flash column chromatography was performed using 230–400 mesh Kieselgel 60 silica eluting with analytical grade solvents. Commercial materials were used a received unless otherwise noted. Amino acids, coupling reagents and resins were obtained from Novabiochem. Dichloromethane and methanol were distilled from calcium hydride. DMF was obtained as peptide synthesis grade from Auspep or Labscan.

2.2. Synthesis of bisubstrate conjugates

2.2.1. Synthesis of 2',3'-O-isopropylideneuridine

To a stirred solution of uridine (3, 10.0 g, 41.0 mmol) and *p*-toluenesulfonic acid (0.779 g, 4.10 mmol) in acetone (100 mL) was added 2,2-dimethoxypropane (6.40 g, 61.4 mmol) under argon. The mixture was stirred at 60 $^{\circ}\text{C}$ for 24 h before being concentrated under reduced pressure. The crude material was purified by flash chromatography (1:9 v/v MeOH/DCM) to yield the title compound (11.2 g, 96%) as a white foam; mp. 169 $^{\circ}\text{C}$; ^1H NMR (500 MHz, CD_3OD): δ 7.78 (d, $J = 8.1$ Hz, 1H), 5.86 (d, $J = 2.8$ Hz, 1H), 5.50 (d, $J = 8.0$ Hz, 1H) 4.96 (dd, $J = 2.8$, 6.3 Hz, 1H), 4.63 (dd, $J = 3.4$, 6.3 Hz, 1H), 4.22 (m, 1H), 3.75 (dd, $J = 3.6$, 11.9 Hz, 1H), 3.72 (dd, $J = 4.5$, 11.9 Hz, 1H), 1.54 (s, 3H), 1.30 (s, 3H); ^{13}C NMR (100 MHz, CD_3OD): δ 166.8, 153.1, 144.5, 113.1, 101.6, 92.5, 88.5, 85.6, 82.4, 62.1, 26.7, 25.5. Data are in agreement with that

previously reported [39].

2.2.2. Synthesis of 2',3'-O-isopropylidene-5'-O-toluenesulfonyluridine

To 2',3'-O-isopropylideneuridine (2.50 g, 8.79 mmol) dissolved in pyridine (15.0 mL) at 0 $^{\circ}\text{C}$ over an hour. After, 4-toluenesulfonyl chloride (4.67 g, 24.6 mmol) and DMAP (0.247 g, 2.02 mmol) were added and mixed at room temperature over 48 h. The mixture was diluted with water (100 mL) and extracted with ethyl acetate (3 \times 100 mL). The combined organic fractions were washed with 0.1 M hydrochloric acid (50.0 mL) before water (100 mL) and finally brine (100 mL) before drying (Na_2SO_4) and concentrating under reduced pressure. The crude material was a yellow oil and was purified by flash chromatography (1:5 v/v Hex/EtOAc) to yield the title compound (2.85 g, 74%) as a pale yellow foam; mp 93 $^{\circ}\text{C}$; ^1H NMR (500 MHz, CDCl_3): δ 9.93 (s, 1H) 7.71 (d, $J = 8.2$ Hz, 2H), 7.28 (d, $J = 8.0$ Hz, 2H), 7.22 (d, $J = 8.1$ Hz, 1H), 5.66 (d, $J = 8.0$ Hz, 1H), 5.6 (d, $J = 2.0$, 1H), 4.90 (dd, $J = 1.9$, 6.4 Hz, 1H), 4.74 (dd, $J = 3.8$, 6.4 Hz, 1H), 4.25–2.33 (m, 1H), 4.21–4.28 (m, 2H) 2.29 (s, 3H) 1.44 (s, 3H), 1.23 (s, 3H); ^{13}C NMR (100 MHz, CDCl_3): δ 163, 150, 145, 143, 133, 130, 128, 115, 103, 95.0, 85.2, 84.4, 80.9, 69.5, 27.1, 25.2, 21.7. Data are in agreement with that previously reported [40].

2.2.3. Synthesis of 5'-azido-5'-deoxy-2',3'-O-isopropylideneuridine

To a stirred solution of 2',3'-O-isopropylidene-5'-O-toluenesulfonyluridine (3.76 g, 8.00 mmol) in DMF (15.0 mL) was added sodium azide (0.779 g, 12.0 mmol) under argon at room temperature. The mixture was heated to 80 $^{\circ}\text{C}$ and stirred for 24 h. The mixture was diluted with water (100 mL) and extracted with ethyl acetate (3 \times 100 mL). The combined organic layers were washed with brine before drying (Na_2SO_4) and concentrating under reduced pressure. The crude material was purified by flash chromatography (2:3 v/v Hex/EtOAc) to yield the title compound (2.30 g, 97%) as an amorphous yellow foam; ν_{max} 3 (film)/ cm^{-1} 219, 2985, 2106, 1677, 1538, 1461, 1375, 1260, 1154, 1091; ^1H NMR (300 MHz, CDCl_3): δ 8.76 (s, 1H), 7.30 (d, $J = 8.0$ Hz, 1H), 5.75 (d, $J = 8.0$ Hz, 1H), 5.65 (d, $J = 2.1$ Hz, 1H), 4.99 (dd, $J = 2.0$, 6.5 Hz, 1H), 4.81 (dd, $J = 4.2$, 6.5 Hz, 1H), 4.21–4.24 (m, 1H) 3.60 (dd, $J = 5.2$ Hz, 2H), 1.45 (s, 3H), 1.24 (s, 3H); ^{13}C NMR (100 MHz, CDCl_3): δ 164, 150, 143, 115, 103, 94.9, 86.0, 84.4, 81.6, 52.4, 27.1, 25.3. Data are in agreement with that previously reported [40].

2.2.4. Synthesis of 5'-amino-5'-deoxy-2',3'-O-isopropylideneuridine (4)

To a stirred solution of 5'-azido-5'-deoxy-2',3'-O-isopropylideneuridine (2.75 g, 9.64 mmol) in methanol (50.0 mL) was added Pd/C (0.275 g, 10% w/w) under argon at 10 $^{\circ}\text{C}$. The mixture was then bubbled with hydrogen gas at room temperature and the progress of the reaction was monitored closely by TLC analysis. After completion, the reaction mixture was filtered through a Celite[®] bed, washed with cold methanol, and concentrated under reduced pressure to afford the title compound (2.39 g, 95%) as a white powder which was not purified further; mp. 85 $^{\circ}\text{C}$; ^1H NMR (300 MHz, $\text{DMSO}-d_6$): δ 7.85 (d, $J = 8.1$ Hz, 1H), 5.78 (d, $J = 2.8$ Hz, 1H), 5.63 (d, $J = 8.0$ Hz, 1H), 4.94 (dd, $J = 6.4$, 2.8 Hz, 1H), 4.74 (dd, $J = 6.5$, 3.9 Hz, 1H), 3.94 (m, 1H), 3.19 (br, s, 2H), 2.75 (d, $J = 5.5$ Hz, 2H), 1.44 (s, 3H), 1.26 (s, 3H). Data are in agreement with that previously reported [40].

2.2.5. Synthesis of Boc-6-aminocaproic acid

To a solution of 6-aminocaproic acid (1, 3.00 g, 22.9 mmol) and NaOH (0.930, 25.2 mmol) in dioxane/ H_2O (90.0 mL, 2:1) was added di-*tert*-butyl dicarbonate (5.49 g, 25.2 mmol) at 0 $^{\circ}\text{C}$ in three equal portions. The reaction mixture was stirred for 16 h before being concentrated under reduced pressure. The residue was redissolved in H_2O (150 mL) and washed with ethyl acetate (2 \times 90.0 mL) before being acidified to pH 2 with aqueous 1 M HCl. The aqueous phase was then extracted with ethyl acetate (3 \times 150 mL) after which the organic phase was dried with Na_2SO_4 , filtered and concentrated under reduced pressure to yield the title compound (5.29 g, quant.) as a colourless oil; ^1H NMR (300

MHz, CDCl₃): δ 3.09 (m, 2H), 2.34 (t, $J = 7.5$ Hz, 2H), 1.65 (m, 2H), 1.49 (m, 2H), 1.46 (s, 9H), 1.37 (m, 2H). Data are in agreement with that previously reported [41].

2.2.6. Synthesis of benzyl-6-(Boc-*N*-amino)hexanoate

To a solution of Boc-6-aminocaproic acid (5.42 g, 23.4 mmol) in DCM (150 mL) was added EDC (4.93 g, 25.7 mmol), benzyl alcohol (30.4 mmol, 3.16 mL) and DMAP (0.286 g, 2.34 mmol) at 0 °C. The reaction mixture was allowed to warm to room temperature and was stirred for 16 h before being quenched by addition of saturated NH₄Cl (100 mL) solution. The mixture was extracted with ethyl acetate (3 × 150 mL), washed with brine (25 mL) and dried over Na₂SO₄ before being concentrated under reduced pressure and purified by flash chromatography (1:3 EtOAc/Hex) yielding the title compound (7.51 g, quant.) as a yellow oil; ¹H NMR (300 MHz, CDCl₃): δ 7.32 (m, 5H), 5.08 (s, 2H), 4.63 (br, 1H), 3.20 (m, 2H) 2.35 (t, $J = 7.4$ Hz, 2H), 1.64 (m, 4H), 1.56 (s, 9H), 1.37 (m, 2H). Data are in agreement with that previously reported [42].

2.2.7. Synthesis of benzyl-6-aminohexanoate

To a mixture of benzyl-6-(Boc-*N*-amino)hexanoate (7.50 g, 23.4 mmol) in DCM (120 mL) was added TFA (60.0 mL) at 0 °C with stirring. After 2 h, the mixture was concentrated under reduced pressure, after which the residue was redissolved in saturated NaHCO₃ solution (100 mL) and extracted with ethyl acetate (3 × 120 mL). The mixture was concentrated under reduced pressure to yield the title compound (5.16 g, quant.) as a yellow wax requiring no further purification; ¹H NMR (300 MHz; CD₃OD): δ 7.36 (m, 5H), 5.13 (s, 2H), 2.91 (t, $J = 1.6$ Hz, 2H) 2.42 (t, $J = 7.3$ Hz, 2H), 1.64 (m, 4H), 1.56 (s, 9H), 1.37 (m, 2H). Data are in agreement with that previously reported [42].

2.2.8. Synthesis of 2-diethoxy-1-cyclobutene-3,4-dione

To a stirred solution of 3,4-dihydroxycyclobut-3-ene-1,2-dione (3.00 g, 26.4 mmol) in anhydrous ethanol (150 mL) was added triethyl orthoformate (72.2 mmol, 12.0 mL) at room temperature. The mixture was heated to reflux at 80 °C and left for 48 h before being concentrated under reduced pressure. The crude yellow oil was purified by flash chromatography (DCM) to yield the title compound (3.57 g, 97%) as an intensely yellow oil which was not purified further; ¹H NMR (300 MHz, CDCl₃): δ 4.72 (m, 4H), 1.44 (t, $J = 87.9$ Hz, 6H). Data are in agreement with that previously reported [43].

2.2.9. Synthesis of benzyl 6-[(2-ethoxy-3,4-dioxo-1-cyclobuten-1-yl)amino]hexanoate (2)

To a stirred solution of 1,2-diethoxy-1-cyclobutene-3,4-dione (3.40 g, 20.0 mmol) in ethanol (70 mL) was portionally added benzyl-6-aminohexanoate (4.42 g, 20.0 mmol) on ice. After 30 min, DIPEA (20.0 mmol, 2.80 mL) was added and the mixture was allowed to reach room temperature and the reaction was monitored by TLC. Upon completion, the reaction mixture was concentrated under reduced pressure before being purified by flash chromatography (1:1 v/v Hex/EtOAc) to yield the title compound (6.62 g, 96%) as a pale-yellow wax; mp. 52 °C; ν_{\max} (film)/cm⁻¹ 3264, 2938, 1803, 1793, 1594, 1523, 1493, 1454, 1414, 1383, 1337, 1235, 1057; ¹H NMR (500 MHz, CDCl₃): δ 7.32 (m, 5H), 5.09 (s, 2H), 4.74 (q, $J = 6.9$, 6.3 Hz, 2H), 3.4 (d, $J = 6.8$ Hz, 1H), 2.35 (t, $J = 7.4$ Hz, 2H), 1.64 (m, 4H), 1.42 (t, $J = 7.0$ Hz, 3H), 1.37 (m, 2H); ¹³C NMR (126 MHz, CDCl₃): δ 189.25, 182.37, 176.86, 172.99, 172.36, 135.73, 128.23, 127.88, 127.81, 69.30, 65.82, 44.25, 33.71, 29.82, 25.47, 24.04, 15.55; HRMS (ESI) 368.14710 ([M + Na]⁺), calcd. for C₁₉H₂₃NNaO₅⁺ 368.14684.

2.2.10. Synthesis of benzyl 6-[(2-(5'-amino-5'-deoxy-2',3'-O-isopropylideneuridine)-3,4-dioxo-1-cyclobuten-1-yl)amino]hexanoate (5)

To a solution of benzyl 6-[(2-ethoxy-3,4-dioxo-1-cyclobuten-1-yl)amino]hexanoate 2 (2.91 g, 8.45 mmol) and 5'-amino-5'-deoxy-2',3'-O-isopropylideneuridine 4 (2.39 g, 8.45) in ethanol (25 mL) was added

DIPEA (25.3 mmol, 3.55 mL) with stirring at room temperature. The reaction mixture was left for 48 h after which it had formed a thick white precipitate. The mix was concentrated under reduced pressure, and the impurities were decanted with ethyl acetate to yield the title compound (4.28 g, 87%) as a white foam; ν_{\max} (solid)/cm⁻¹ 3162, 2942, 1734, 1712, 1689, 1637, 1571, 1487, 1441, 1304, 1071; ¹H NMR (500 MHz, DMSO-*d*₆): δ 11.4 (s, 1H), 7.70 (d, $J = 7.8$ Hz, 1H), 7.35 (m, 5H), 5.80 (s, 1H), 5.62 (d, $J = 7.8$ Hz, 1H) 5.07 (s, 2H) 5.05 (d, $J = 1.5$ Hz, 1H), 4.75 (t, $J = 5.1$ Hz, 1H), 4.07 (dd, $J = 5.05$ Hz, 1H), 3.86 (br, 1H), 3.70 (m, 1H), 3.46 (d, $J = 5.1$ Hz, 2H), 2.36 (t, $J = 7.2$ Hz, 2H) 1.53 (m, 4H), 1.47 (s, 3H), 1.28 (m, $J = 8.4$ Hz, 2H), 1.28 (s, 3H); ¹³C NMR (126 MHz, DMSO-*d*₆): δ 182.7, 182.2, 172.7, 167.5, 163.2, 150.2, 143.1, 136.2, 128.4, 127.9, 127.9, 113.5, 101.9, 92.2, 85.5, 83.4, 80.9, 65.3, 45.1, 43.1, 33.3, 30.3, 26.9, 25.5, 25.2, 24; HRMS (ESI) 605.22131 ([M + Na]⁺), calcd. for C₂₉H₃₄N₄NaO₉⁺ 605.22180.

2.2.11. Synthesis of 6-[(2-(5'-amino-5'-deoxy-2',3'-O-isopropylideneuridine)-3,4-dioxo-1-cyclobuten-1-yl)amino]hexanoic acid (6)

To a solution of benzyl 6-[(2-(5'-amino-5'-deoxy 2',3'-O-isopropylideneuridine)-3,4-dioxo-1-cyclobuten-1-yl)amino]hexanoate 5 (2.00 g, 3.44 mmol) in methanol (30.0 mL) was added 1 M sodium hydroxide solution (20.0 mL) and stirred at rt. The reaction was kept at pH greater than 14 and was monitored by TLC. Upon completion, the reaction was treated with Amberlite® IR 120H⁺ resin until pH 4. The mixture was filtered and concentrated under reduced pressure. To this dry mixture was suspended into ethyl acetate and once settled the supernatant was decanted and re-dried to yield the title compound (1.46 g, quant.) as a pale yellow powder; ν_{\max} cm⁻¹ 2939, 1648, 1564, 1433, 1270, 1061; ¹H NMR (500 MHz, DMSO-*d*₆): δ 7.65 (d, $J = 8.0$ Hz, 1H), 5.77 (s, 1H), 5.59 (d, $J = 7.9$ Hz, 1H), 5.59 (d, $J = 7.9$ Hz, 1H), 4.72 (s, 1H), 4.07 (app, 1H), 3.86 (app, 1H), 3.70 (app, 1H), 3.46 (app, 2H), 2.17 (t, $J = 7.2$ Hz, 2H), 1.47 (m, 4H), 1.44 (3H), 1.25 (m, 4H), 1.24 (s, 1H); ¹³C NMR (126 MHz, DMSO-*d*₆): δ 183.2, 182.7, 175.2, 168.5, 164.0, 150.9, 143.8, 114.3, 102.5 92.7, 86.3, 84.0, 81.5, 45.7, 43.8, 34.1, 31.0, 27.5, 25.7, 25.4, 24.7; HRMS (ESI) 449.18933 ([M + Na]⁺), calcd. for C₂₀H₃₀N₂NaO₈⁺ 449.18944.

2.2.12. Synthesis of 1-(2-bromoethyl)-2-acetamido-2-deoxy- α -D-glucopyranoside

To 2-bromoethanol (30.0 mL) was added acetyl chloride (46.1 mmol, 3.30 mL) dropwise at 0 °C with mixing under argon. To this mixture, *N*-acetylglucosamine (7, 3.00 g, 13.6 mmol) was added before heating to 70 °C for 4 h. After, solid sodium bicarbonate was added until pH 7 and the suspension was filtered through a celite bed and washed with methanol. The mixture was concentrated under reduced pressure before purification by flash chromatography (1:5 MeOH/DCM) to give the title compound (2.618 g, 55%) as a light brown powder; ¹H NMR (500 MHz, CD₃OD): δ 4.82 (d, $J = 4.0$ Hz, 1H), 3.98 (m, 1H), 3.91 (dd, $J = 13.5$, 4.5 Hz, 1H), 3.79 (m, 2H), 3.66 (m, 2H), 3.61 (m, 2H), 3.37 (m, 1H), 3.31 (t, $J = 2.1$ Hz, 1H), 2.01 (s, 3H); ¹³C NMR (126 MHz, CD₃OD): δ 172, 97.8, 72.6, 71.7, 68.4, 60.9, 54.2, 47.5, 29.9, 21.0. Data are in agreement with that previously reported [44].

2.2.13. Synthesis of 1-(2-azidoethyl)-2-acetamido-2-deoxy- α -D-glucopyranoside

To a solution of 1-(2-bromoethyl)-2-acetamido-2-deoxy- α -D-glucopyranoside (2.13 g, 6.10 mmol) in acetone/H₂O (1:1 v/v, 20 mL) was added sodium azide (2.379 g, 36.60 mmol) and tetrabutylammonium iodide (2.275 g, 6.16 mmol) under argon. The mixture was then stirred at 60 °C for 24 h, before being concentrated under reduced pressure and purified by flash chromatography (1:5 v/v MeOH/DCM) to give the title compound (0.956 g, quant.) as an amorphous yellow foam; ¹H NMR (400 MHz, CD₃OD): δ 4.88 (d, $J = 3.6$ Hz, 1H), 3.91 (m, 2H), 3.84 (dd, $J = 11.9$, 2.5 Hz, 1H), 3.73 (m, 2H), 3.63 (m, 2H) 3.44 (m, 2H), 3.33 (m, 1H), 2.01 (s, 3H); ¹³C NMR (101 MHz, MD₃OD): δ 172.37, 97.42, 72.51,

71.35, 70.73, 66.51, 61.29, 53.85, 50.42, 21.79. Data are in agreement with that previously reported [44].

2.2.14. Synthesis of 1-(2-aminoethyl)-2-acetamido-2-deoxy- α -D-glucopyranoside (**8**)

To a solution of 1-(2-azidoethyl)-2-acetamido-2-deoxy- α -D-glucopyranoside (0.63 g, 2.17 mmol) in methanol was added Pd/C (63 mg, 10% w/w) in methanol (15 mL) under argon. The solution was bubbled with H₂ gas from a balloon with stirring for 24 h. The mixture was then filtered through a celite bed and washed with cold methanol before being concentrated under reduced pressure. The crude material was a light-yellow foam (0.4979 g, 87%) and was used without further purification. ν_{\max} (film)/cm⁻¹ 3287, 2905, 1688, 1615, 1594, 1333, 1209, 1029; ¹H NMR (400 MHz, CD₃OD): δ 4.79 (d, *J* = 3.6 Hz), 3.96 (m, 2H), 3.85 (dd, *J* = 11.8, 2.3, 1H), 3.74 (m, 2H), 3.65 (m, 2H), 3.39 (m, 2H), 2.89 (m, 1H), 2.02 (s, 3H); ¹³C NMR (101 MHz, CD₃OD): δ 172.3, 97.5, 72.5, 71.6, 70.9, 68.5, 61.3, 53.9, 40.6, 21.3; HRMS (ESI) 287.12165 ([M + Na]⁺), calcd. for C₁₀H₂₀N₂NaO₆⁺ 287.12136.

2.2.15. Synthesis of 1-[benzyl [6-(2'-aminoethyl)-3,4-dioxo-1-cyclobuten-1-yl]amino]hexanoate]-2-acetamido-2-deoxy- α -D-glucopyranoside (**9**)

To a solution of benzyl 6-[(2-ethoxy-3,4-dioxo-1-cyclobuten-1-yl)amino]hexanoate **2** (0.819 g, 2.075 mmol) in ethanol (10 mL) was added 1-(2-aminoethyl)-2-acetamido-2-deoxy- α -D-glucopyranoside **8** (0.498 g, 1.89 mmol) with stirring at room temperature. After 15 min, DIPEA (5.657 mmol, 0.571 mL) was added and the solution was left stirring for 48 h after which it had formed a thick white precipitate. The mixture was concentrated under reduced pressure and the impurities were decanted with ethyl acetate to yield the title compound (0.773 g, 73%) as a colourless foam; ν_{\max} (film)/cm⁻¹ 3333, 2929, 1727, 1660, 1605, 1554 1310, 1133, 1048; ¹H NMR (500 MHz, DMSO-*d*₆): δ 7.44 (d, *J* = 8.6 Hz, 1H), 7.35 (m, 5H) 5.09 (s, 2H), 5.00 (d, *J* = 5.3 Hz, 1H) 4.77 (d, *J* = 5.5 Hz, 1H), 4.67 (d, *J* = 3.6 Hz, 1H), 4.53 (t, *J* = 5.9 Hz, 1H), 3.65 (m, 4H), 3.47 (m, 4H), 3.16 (dd, *J* = 9.9, 4.3 Hz, 1H), 2.37 (t, *J* = 7.4 Hz, 2H), 1.84 (s, 3H), 1.55 (m, 4H), 1.31 (m, 2H); ¹³C NMR (126 MHz, DMSO-*d*₆): δ 183, 183, 173, 170, 168, 168, 137, 129, 128, 128, 97.9, 73.4, 71.3, 71.1, 67.7, 65.8, 61.2, 54.0, 49.1, 43.6, 43.5, 33.8, 30.9, 25.8, 24.5, 23.3, 20.9; HRMS (ESI) 586.23742 ([M + Na]⁺), calcd. for C₂₇H₃₇N₃NaO₁₀⁺ 586.23712.

2.2.16. Synthesis of 1-[6-(2'-aminoethyl)-3,4-dioxo-1-cyclobuten-1-yl]amino]hexanoic acid]-2-acetamido-2-deoxy- α -D-glucopyranoside (**10**)

To a solution of 1-[benzyl [6-(2-aminoethyl)-3,4-dioxo-1-cyclobuten-1-yl]amino]hexanoate]-2-acetamido-2-deoxy- α -D-glucopyranoside **9** (0.725 g, 1.29 mmol) in methanol was added Pd/C (0.0725 g, 10% w/w) in methanol (15 mL) under argon. The solution was bubbled with H₂ gas from a balloon with stirring for 24 h. The mixture was then filtered through a celite bed and washed with cold methanol before being concentrated under reduced pressure. The crude material was a pale-yellow foam (0.533 g, 88%) and was used as such without further purification. ν_{\max} (film)/cm⁻¹ 3246, 2932, 1650, 1588, 1535, 1431, 1342, 1122, 1022; ¹H NMR (500 MHz, CD₃OD): δ 4.80 (d, *J* = 3.5 Hz, 1H), 3.92 (dd, *J* = 10.5, 3.6 Hz, 1H), 3.83 (m, 3H), 3.65 (m, 7H), 2.30 (t, *J* = 7.4 Hz, 2H), 2.02 (s, 3H), 1.64 (m, 4H), 1.43 (m, 2H); ¹³C NMR (126 MHz, CD₃OD): δ 181.62, 181.46, 185.68, 171.77, 167.66, 167.51, 96.87, 72.08, 70.89, 70.09, 66.72, 60.66, 53.12, 43.34, 42.99, 32.91, 29.81, 24.96, 23.63, 20.90; HRMS (ESI) 496.19034 ([M + Na]⁺), calcd. for C₂₀H₃₁N₃NaO₁₀⁺ 496.19017.

2.3. Solid-phase synthesis protocol (100 μ mol scale)

Solid-phase synthesis of peptide and glycopeptide were carried out manually in disposable Torviq polypropylene syringes equipped with Teflon sinter.

2.3.1. Loading of amino acid onto Rink amide (RAM) resin (100 μ mol scale)

SPPS was conducted using established protocols [45]. Rink amide (RAM) resin (0.41 mmol/g loading, 244 mg, 0.1 mmol) was swollen in dry DMF (3 mL) for 5 min at room temperature before being treated with piperidine in DMF (4 mL, 10% v/v) solution and shaken for 5 min at room temperature. The procedure was repeated with a fresh portion of deprotection mixture, after which the resin was washed with DMF (5 \times 5 mL), DCM (5 \times 2 mL) and then DMF (5 \times 2 mL). After, a solution of the Fmoc-protected amino acid (400 μ mol, 4 equiv.), PyBOP (400 μ mol, 4 equiv.) and NMM (800 μ mol, 8 equiv.) in DMF (1 mL) was mixed with the resin and shaken for 1 h. After, the resin was washed with DMF (5 \times 2 mL), DCM (5 \times 2 mL) and then DMF (5 \times 2 mL). Each desired sequence was then assembled manually following the general procedure.

2.3.2. Determination of resin loading

A solution of piperidine in DMF (4 mL, 10% v/v) was added to the resin, which was shaken for 3 min and procedure repeated. The drained Fmoc deprotection solution was retained in a 10 mL volumetric flask and the resin washed with fresh piperidine in DMF (10% v/v) such that the total volume did not exceed 10 mL. The efficiency of the initial loading was quantitatively determined by measurement of the dibenzofulvene-piperidine adduct using Varian Cary 4000 UV-Vis spectrophotometer (λ = 301 nm). Amino acid loading onto the resin was quantitative. The resin was subsequently washed with DMF (10 \times 5 mL), DCM (10 \times 5 mL), and DMF (10 \times 5 mL).

2.3.3. Capping

Acetic anhydride/pyridine (1:9 v/v, 2 mL) was added to the resin and shaken. After 3 min the resin was washed with DMF (5 \times 5 mL), DCM (5 \times 5 mL) and DMF (5 \times 5 mL).

2.3.4. Fmoc deprotection

The resin was treated with a solution of piperidine in DMF (4 mL, 10% v/v) and shaken for 3 min. at rt. The procedure was repeated with a fresh portion of deprotection mixture after which the resin was washed with DMF (5 \times 5 mL), DCM (5 \times 5 mL), and DMF (5 \times 5 mL).

2.3.5. Amino acid coupling

A solution of protected amino acid (4 equiv), benzotriazole-1-yl-oxyl-tris-pyrrolidino-phosphonium hexafluorophosphate (PyBOP) (416 mg, 0.8 mmol, 4 equiv), and *N*-methylmorpholine (NMM) (176 μ L, 1.6 mmol, 8 equiv) in DMF (2.5 mL) was added to the resin and shaken. After 1 h the resin was washed with DMF (5 \times 5 mL), DCM (5 \times 5 mL), and DMF (5 \times 5 mL).

2.3.6. Resin cleavage

The resin was treated with a solution of TFA/TIS/H₂O (90:5:5, 1 mL) and was shaken for 2 h at room temperature. After, the resin was washed with TFA (2 \times 2 mL) and the resultant mixture was blow dried with nitrogen, redissolved in a mixture of H₂O/MeCN (1:1, 1 mL), and finally lyophilised affording a free flowing, crude mixture. This was then redissolved in H₂O (3 mL), filtered, and analysed by LCMS to provide a trace for preparative RP-HPLC of the filtered mixture.

2.3.7. Squaramide-linked uridine-peptide conjugate assembly protocol

Following the general Fmoc-strategy procedure outlined prior, the appropriate resin-bound sequence was subject to a final Fmoc deprotection step. Following washing, the resin was treated with a coupling solution comprised of the squaramide-linked derivative **6** (0.0221 g, 45.0 μ mol, 1.5 equiv.), coupling reagent HATU (0.024 g, 120 μ mol, 4 equiv.) and NMM (240 μ mol, 8 equiv.) in DMF (1 mL) and shaken for 24 h at room temperature. After, the resin was washed with DMF (5 \times 2 mL), DCM (5 \times 2 mL) and then DMF (5 \times 2 mL). An *in situ* resin cleavage was conducted and the contents of the mixture were identified. After, the cleavage procedure was conducted on a large scale, the resultant

solid was purified by preparative RP-HPLC.

2.3.8. Squaramide-linked GlcNAc-peptide conjugate assembly protocol

Following the general Fmoc-strategy procedure outlined prior, the appropriate resin-bound sequence was subject to a final Fmoc deprotection step. Following washing, the resin was treated with a coupling solution comprised of the squaramide-linked derivative **10** (0.0284 g, 60.0 μmol , 2 equiv.), coupling reagent HATU (0.024 g, 120 μmol , 4 equiv.) and NMM (240 μmol , 8 equiv.) in DMF (1 mL) and shaken for 24 h at room temperature. After, the resin was washed with DMF (5 \times 2 mL), DCM (5 \times 2 mL) and then DMF (5 \times 2 mL). An *in situ* resin cleavage was conducted and the contents of the mixture were identified. After, the cleavage procedure was conducted on a large scale, the resultant solid was purified by preparative RP-HPLC.

2.3.9. Synthesis of (6-[(2-(5'-amino-5'-deoxy-2',3'-O-isopropylideneuridine)-3,4-dioxo-1-cyclobuten-1-yl)amino]hexanoyl)-Ala-Ile-Pro-Val-Ser-Arg-Ala-Glu-Lys-NH₂ (**22**)

Resin-bound peptide (Fmoc-Ala-Ile-Pro-Val-Ser-Arg-Ala-Glu-Lys) (30.0 μmol) was reacted with squaramide-linked uridine derivative **6** following the general squaramide-linked uridine-peptide conjugate assembly protocol outlined prior, purified by preparative RP-HPLC and lyophilised to give the title compound as a white solid (19.4 mg, 46%). LCMS: $R_t = 11$ min (0–50% over 30 min); HRMS: (ESI) 702.36725 ([M + 2H]²⁺), calcd. for C₆₁H₁₀₀N₁₈O₂₀²⁺ 702.36752.

2.3.10. Synthesis of (6-[(2-(5'-amino-5'-deoxy-2',3'-O-isopropylideneuridine)-3,4-dioxo-1-cyclobuten-1-yl)amino]hexanoyl)-Arg-Ile-Pro-Val-Ser-Arg-Ala-Glu-Lys-NH₂ (**23**)

Resin-bound peptide (Fmoc-Arg-Ile-Pro-Val-Ser-Arg-Ala-Glu-Lys) (30.0 μmol) was reacted with squaramide-linked uridine derivative **6** following the general squaramide-linked uridine-peptide conjugate assembly protocol outlined prior, purified by preparative RP-HPLC and lyophilised to give the title compound as a white solid (16.6 mg, 37%). LCMS: $R_t = 9$ min (0–50% over 30 min); HRMS: (ESI) 744.89969 ([M + 2H]²⁺), calcd. for C₆₄H₁₀₇N₂₁O₂₀²⁺ 744.89951.

2.3.11. Synthesis of (6-[(2-(5'-amino-5'-deoxy-2',3'-O-isopropylideneuridine)-3,4-dioxo-1-cyclobuten-1-yl)amino]hexanoyl)-Ala-Leu-Pro-Val-Ser-Arg-Ala-Glu-Lys-NH₂ (**24**)

Resin-bound peptide (Fmoc-Ala-Leu-Pro-Val-Ser-Arg-Ala-Glu-Lys) (30.0 μmol) was reacted with squaramide-linked uridine derivative **6** following the general squaramide-linked uridine-peptide conjugate assembly protocol outlined prior, purified by preparative RP-HPLC and lyophilised to give the title compound as a white solid (12.7 mg, 30%). LCMS: $R_t = 11$ min (0–50% over 30 min); HRMS: (ESI) 702.36768 ([M + 2H]²⁺), calcd. for C₆₁H₁₀₀N₁₈O₂₀²⁺ 702.36752.

2.3.12. Synthesis of (6-[(2-(5'-amino-5'-deoxy-2',3'-O-isopropylideneuridine)-3,4-dioxo-1-cyclobuten-1-yl)amino]hexanoyl)-Ala-Ile-Pro-Val-Ser-Lys-Ala-Glu-Lys-NH₂ (**25**)

Resin-bound peptide (Fmoc-Ala-Ile-Pro-Val-Ser-Lys-Ala-Glu-Lys) (30.0 μmol) was reacted with squaramide-linked uridine derivative **6** following the general squaramide-linked uridine-peptide conjugate assembly protocol outlined prior, purified by preparative RP-HPLC and lyophilised to give the title compound as a white solid (3.30 mg, 8%). LCMS: $R_t = 10$ min (0–50% over 30 min); HRMS: (ESI) 688.36499 ([M + 2H]²⁺), calcd. for C₆₁H₁₀₀N₁₈O₂₁²⁺ 688.36444.

2.3.13. Synthesis of (6-[(2-(5'-amino-5'-deoxy-2',3'-O-isopropylideneuridine)-3,4-dioxo-1-cyclobuten-1-yl)amino]hexanoyl)-Ala-Ile-Pro-Val-Ser-Arg-Ala-Asp-Lys-NH₂ (**26**)

Resin-bound peptide (Fmoc-Ala-Ile-Pro-Val-Ser-Arg-Ala-Asp-Lys) (30.0 μmol) was reacted with squaramide-linked uridine derivative **6** following the general squaramide-linked uridine-peptide conjugate assembly protocol outlined prior, purified by preparative RP-HPLC and

lyophilised to give the title compound as a white solid (14.5 mg, 35%). LCMS: $R_t = 11$ min (0–50% over 30 min); HRMS: (ESI) 695.35999 ([M + 2H]²⁺), calcd. for C₆₀H₉₈N₁₈O₂₀²⁺ 695.35969.

2.3.14. Synthesis of (6-[(2-(5'-amino-5'-deoxy-2',3'-O-isopropylideneuridine)-3,4-dioxo-1-cyclobuten-1-yl)amino]hexanoyl)-Ala-Ile-Pro-Val-Ser-Arg-Pro-Glu-Lys-NH₂ (**27**)

Resin-bound peptide (Fmoc-Ala-Ile-Pro-Val-Ser-Arg-Pro-Glu-Lys) (30.0 μmol) was reacted with squaramide-linked uridine derivative **6** following the general squaramide-linked uridine-peptide conjugate assembly protocol outlined prior, purified by preparative RP-HPLC and lyophilised to give the title compound as a white solid (10.9 mg, 25%). LCMS: $R_t = 11$ min (0–50% over 30 min); HRMS: (ESI) 715.37545 ([M + 2H]²⁺), calcd. for C₆₃H₁₀₂N₁₈O₂₀²⁺ 715.37534.

2.3.15. Synthesis of (6-[(2-(5'-amino-5'-deoxy-2',3'-O-isopropylideneuridine)-3,4-dioxo-1-cyclobuten-1-yl)amino]hexanoyl)-Arg-Ile-Pro-Val-Ser-Arg-Pro-Glu-Lys-NH₂ (**28**)

Resin-bound peptide (Fmoc-Arg-Ile-Pro-Val-Ser-Arg-Pro-Glu-Lys) (30.0 μmol) was reacted with squaramide-linked uridine derivative **6** following the general squaramide-linked uridine-peptide conjugate assembly protocol outlined prior, purified by preparative RP-HPLC and lyophilised to give the title compound as a white solid (8.20 mg, 18%). LCMS: $R_t = 9$ min (0–50% over 30 min); HRMS: (ESI) 757.90768 ([M + 2H]²⁺), calcd. for C₆₆H₁₀₉N₂₁O₂₀²⁺ 757.90734.

2.3.16. Synthesis of (6-[(2-(5'-amino-5'-deoxy-2',3'-O-isopropylideneuridine)-3,4-dioxo-1-cyclobuten-1-yl)amino]hexanoyl)-Ala-Pro-Pro-Val-Ser-Arg-Pro-Glu-Lys-NH₂ (**29**)

Resin-bound peptide (Fmoc-Ala-Pro-Pro-Val-Ser-Arg-Pro-Glu-Lys) (30.0 μmol) was reacted with squaramide-linked uridine derivative **6** following the general squaramide-linked uridine-peptide conjugate assembly protocol outlined prior, purified by preparative RP-HPLC and lyophilised to give the title compound as a white solid (11.4 mg, 27%). LCMS: $R_t = 9$ min (0–50% over 30 min); HRMS: (ESI) 707.35999 ([M + 2H]²⁺), calcd. for C₆₂H₉₈N₁₈O₂₀²⁺ 707.35969.

2.3.17. Synthesis of (6-[(2-(5'-amino-5'-deoxy-2',3'-O-isopropylideneuridine)-3,4-dioxo-1-cyclobuten-1-yl)amino]hexanoyl)-Ala-Ile-Pro-Pro-Ser-Pro-Glu-Lys-NH₂ (**30**)

Resin-bound peptide (Fmoc-Ala-Ile-Pro-Pro-Ser-Pro-Glu-Lys) (30.0 μmol) was reacted with squaramide-linked uridine derivative **6** following the general squaramide-linked uridine-peptide conjugate assembly protocol outlined prior, purified by preparative RP-HPLC and lyophilised to give the title compound as a white solid (2.70 mg, 7%). LCMS: $R_t = 12$ min (0–50% over 30 min); HRMS: (ESI) 684.84416 ([M + 2H]²⁺), calcd. for C₆₂H₉₅N₁₅O₂₀²⁺ 684.84334.

2.3.18. Synthesis of (6-[(2-(5'-amino-5'-deoxy-2',3'-O-isopropylideneuridine)-3,4-dioxo-1-cyclobuten-1-yl)amino]hexanoyl)-Val-Pro-Thr-Val-Ser-Thr-Ala-NH₂ (**31**)

Resin-bound peptide (Fmoc-Val-Pro-Thr-Val-Ser-Thr-Ala) (30.0 μmol) was reacted with squaramide-linked uridine derivative **6** following the general squaramide-linked uridine-peptide conjugate assembly protocol outlined prior, purified by preparative RP-HPLC and lyophilised to give the title compound as a white solid (21.4 mg, 64%). LCMS: $R_t = 15$ min (0–50% over 30 min); HRMS: (ESI) 1129.51375 ([M + Na]⁺), calcd. for C₄₈H₇₄N₁₂NaO₁₈⁺ 1129.51362.

2.3.19. Synthesis of (6-[(2-(5'-amino-5'-deoxy-2',3'-O-isopropylideneuridine)-3,4-dioxo-1-cyclobuten-1-yl)amino]hexanoyl)-Ala-Val-Pro-Ser-Thr-Ala-Ser-Thr-NH₂ (**32**)

Resin-bound peptide (Fmoc-Ala-Val-Pro-Ser-Thr-Ala-Ser-Thr) (30.0 μmol) was reacted with squaramide-linked uridine derivative **6** following the general squaramide-linked uridine-peptide conjugate assembly protocol outlined prior, purified by preparative RP-HPLC and

lyophilised to give the title compound as a white solid (8.70 mg, 23%). LCMS: $R_t = 15$ min (0–50% over 30 min); HRMS: (ESI) 655.28614 ($[M + 2Na]^+$), calcd. for $C_{54}H_{84}N_{14}Na_2O_{21}^+$ 655.28599.

2.3.20. Synthesis of 1-[6(2'-aminoethoxy-3,4-dioxo-1-cyclobuten-1-yl)amino]hexanoyl]-Val-Thr-Pro-Val-Ser-Thr-Ala-NH₂]-2-acetamido-2-deoxy- α -D-glucopyranoside (**33**)

Resin-bound peptide (Fmoc-Val-Thr-Pro-Val-Ser-Thr-Ala) (20.0 μ mol) was reacted with squaramide-linked GlcNAc derivative **10** following the general squaramide-linked GlcNAc-peptide conjugate assembly protocol outlined prior, purified by preparative RP-HPLC and lyophilised to give the title compound as a white solid (3.30 mg, 13%). LCMS: $R_t = 15$ min (0–50% over 30 min); HRMS: (ESI) 586.77420 ($[M + 2Na]^+$), calcd. for $C_{49}H_{81}N_{11}Na_2O_{19}^+$ 586.77473.

2.4. Radioactive hOGT assay

Radioactive hOGT assay was performed using recombinant nup62-MBP fusion construct as the protein acceptor and [³H]-UDP-GlcNAc (Specific activity 0.4 Ci/mmol) in 20 μ M total UDP-GlcNAc, 17 μ M nup62, 500 nM hOGT, 12.5 mM MgCl₂ and 20 μ M inhibitor or PBS [46]. The reactions were performed in duplicate and were incubated at 37 °C for 2 h. 20 μ L of each reaction was then applied to 1.5 \times 3 cm strips of nitrocellulose membrane and allowed to air dry. The membranes were added to scintillation vials and washed three times with 3 mL PBS. 4 mL of scintillation fluid (Amersham) was added, and the levels of tritium were quantified in disintegrations per minute (dpm) using a liquid scintillation counter (Beckman LS6000). Inhibition was measured as a percentage of relative OGT activity in the absence of inhibitor.

2.5. Molecular modelling

The crystal structure of hOGT in complex with UDP-GlcNAc [22] was retrieved from Protein Data Bank (PDB code: 4GZ5) and processed by Maestro 11 (Schrödinger, LLC) using default settings. All water molecules in the crystal structures were removed, and only chain A was retained to serve as the receptor molecule in subsequent molecular docking. Structures of ligands in SMILES format were also processed using the LigPrep panel of Maestro 11 (Schrödinger, LLC) with default parameters, and the resulting structures were used as ligands for molecular docking. Induced Fit docking (IFD) [47] that utilizes both Glide [48,49] and Prime refinement [50] functions was performed for all ligands. The grid box was centred on the UDP-GlcNAc of the original crystal structure, which was removed prior to docking. The grid box size was set to 46 \times 46 \times 46 Å, the largest value possible in the graphic user interface of IFD. Other settings were kept as default. The top-ranking docked pose for each ligand was extracted for analyses.

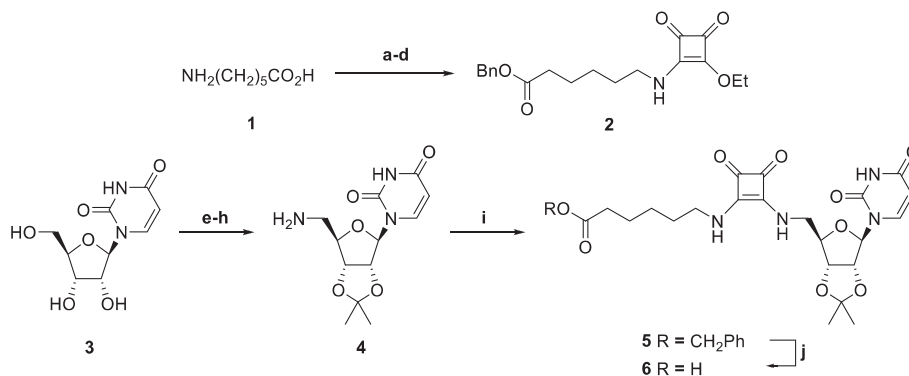
3. Results and discussion

3.1. Synthesis

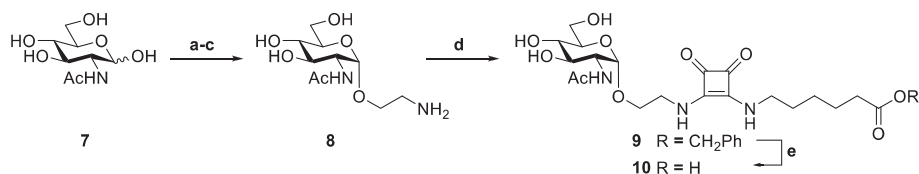
To generate the bisubstrate conjugates, three key precursors building blocks were synthesised, the donor analogue, acceptor analogue, and squaramide tether. An extended aliphatic tether unit was employed to provide the inhibitors with flexibility within the active site. The tether was generated from commercially available 6-aminocaproic acid across five high-yielding steps to produce reactive squaramate **2**, depicted in Scheme 1. Two donor substrate analogues were studied. Uridine was employed as donor substrate analogue, due to its high affinity for OGT. Briefly, commercially available uridine **3** was protected with 2',3'-isopropylidene to allow chemoselective targeting of 5'-hydroxyl. Across three steps, 5'-aminouridine derivative **4** was generated and coupled with squaramate **2** to give squaramide **5**. Finally, base-catalysed hydrolysis of benzyl ester afforded building block **6**.

As GlcNAc has been shown to play a mechanistic role in its own catalytic transfer via UDP-GlcNAc, it was also employed as a candidate donor analogue. Modification of GlcNAc was conducted at the anomeric carbon to mirror the native substrate, as depicted in Scheme 2. The precise conformation of the sugar unit plays a significant role in catalysis. Since GlcNAc exists exclusively in the α -anomer prior to glycosyl-transfer when complexed with UDP, synthesis of the functionalised α -glycoside was pursued. Condensation of GlcNAc (**7**) with 2-bromoethanol yielded the anomer with a 2:1 preference. Initial attempts to produce the building block through installing and conserving 3-, 4- and 6- *O*-acyl groups failed and partial deacetylated intermediates isolated due to basic conditions required in the subsequent coupling steps with squaramate **2**. Synthesis moved forward without acetylation, and although purification and characterisation became more challenging, yields were not compromised. Commercially available GlcNAc was reacted with bromoethanol to produce only the α -anomer of 2'-bromoethoxy-2-acetamido-2-deoxy- α -D-glucopyranoside. The latter was transferred to the 2'-azido derivative, which was subsequently reduced to key intermediate 2-aminoethoxy glucopyranoside **8**. Coupling of **8** with squaramate **2** produced **9** before hydrogenolysis yielded building block **10**. With all building blocks in hand, design and synthesis of the acceptor substrate analogues was conducted.

A limited number of sites of protein *O*-GlcNAcylation have been mapped. Of those, two well-characterised, high-affinity acceptor substrates were selected, i) an α -A crystallin derived peptide (H-Ala-Ile-Pro-Val-Ser-Arg-Glu-Glu-Lys-OH) and ii) the hOGT sequon-derived acceptor substrate Ac-Val-Thr-Pro-Val-Ser-Thr-Ala-NH₂. Both sequences have been studied in this context [26,51,53], their structural conformations and binding interactions with OGT are understood. From these sequences, panels of acceptor substrate analogues containing varying substitutions with various amino acids were designed. Manipulation of



Scheme 1. Synthesis of uridyl-squaramide donor substrate analogue **6**. Reagents and conditions: (a) Boc₂O, NaOH, 1:2 v/v H₂O/dioxane, quant.; (b) BnOH, EDC, DMAP, CH₂Cl₂, quant.; (c) 1:2 v/v CF₃CO₂H/CH₂Cl₂ quant.; (d) **2**, DIPEA, EtOH, 96%; (e) DMP, *p*-TSA, acetone, 90%; (f) *p*-TsCl, DMAP, pyridine, 77%; (g) NaNs, DMF, 97%; (h) H₂, Pd/C (10 wt%) MeOH, 95% (crude); (i) DIPEA, EtOH, 87%; (j) 1 M NaOH, MeOH, quant.



Scheme 2. Synthesis of GlcNAc-squaramide donor substrate analogue **10**. Reagents and conditions: (a) 2-bromoethanol, AcCl, 55%; (b) NaN₃, (Bu)₄Nl, 1:1 v/v H₂O/acetone, quant.; (c) H₂, Pd/C (10 wt%), MeOH, 87%; (d) **2**, Et₃N, EtOH, 73%; (e) H₂, Pd/C (20 wt%), MeOH, 88%.

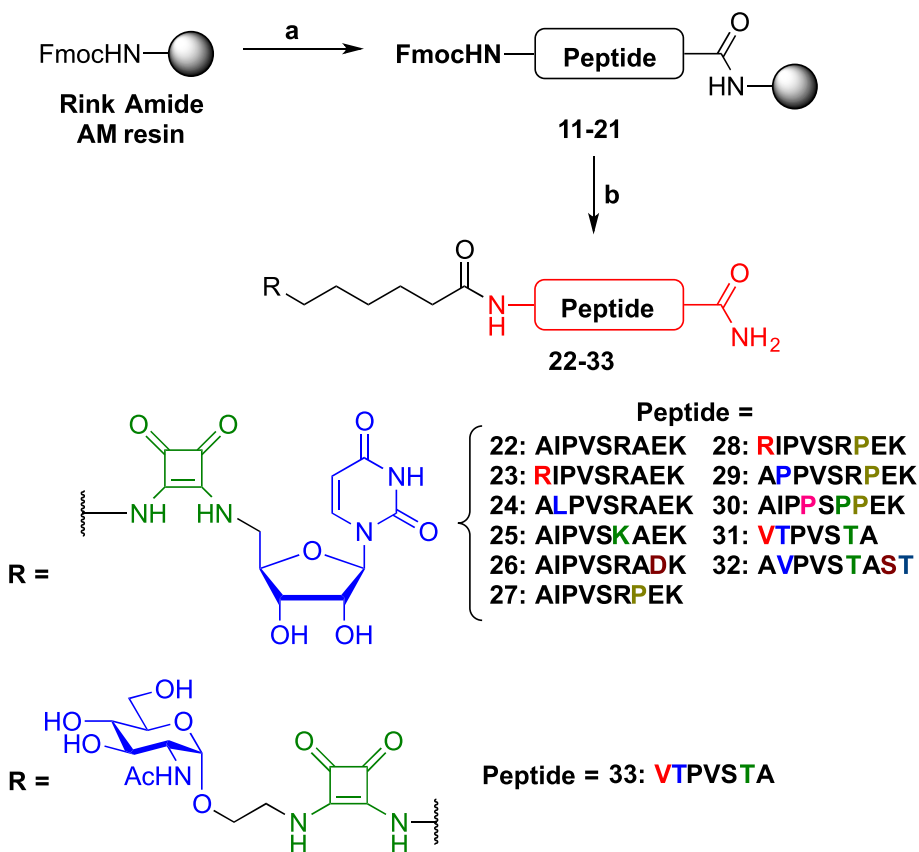
the α -A crystallin sequence via E7A substitution at the +2 subsite produces an acceptor substrate with five-fold affinity increase for OGT [47]. Similarly, A1R substitution at the -4 subsite is suggested to double the activity of the α -A crystallin derived sequence [51]. The effect of increasing stabilisation of the engaged 0 subsite was attempted via incorporation of proline substitutions [52] at nearby, reportedly substitution-tolerant sites [53]. The 'Pro-Val-Ser' (PVS) motif is conserved among the sequences here, as there is a highly conserved 'PVS' motif, thought to be key to OGT's sequence recognition, that exists across the ~50 mapped acceptor sites. Further isosteric substitutions afforded a panel of α -A crystallin derived acceptor substrate analogues.

The acceptor substrates were synthesised using *N*-fluorenylmethoxycarbonyl based solid-phase peptide synthesis (Fmoc-SPPS) using Rink amide (AM) resin and commercially available amino acids and reagents as depicted in Scheme 3. Rink amide resin was used to yield neutrally charged C-terminal carboxamides. Analysis was conducted upon analytical scale aliquots of released crude peptide material to confirm successful construction of the acceptor substrate analogues. Assembly of the peptide-conjugates was conducted on the solid-phase, initiated by removal of peptides *N*-terminal Fmoc group, followed by coupling with the appropriate donor substrate analogue building block **6** or **10**. Reactions were conducted using 1–2 equiv. of donor substrate along with 4M equiv. of 2-(7-aza-1H-benzotriazole-1-yl)-1,1,3,3-

tetramethyluronium hexafluorophosphate (HATU) coupling reagent over 24 h. The conjugates were then released from the solid support under acidic conditions where hydrolysis of the 2',3'-isopropylidene protecting group took place in tandem. The compounds were isolated using reverse phase high-performance liquid chromatography (HPLC), their identities and purity were verified using analytical HPLC and high-resolution mass spectrometry (HRMS).

The inhibitory activities of the bisubstrate analogue inhibitors were examined at 20 μ M concentration using radioactive hOGT assay using recombinant nup62-MBP fusion construct as the protein acceptor and [³H]-UDP-GlcNAc in UDP-GlcNAc as competitive donor substrate. Inhibition was measured as a percentage of relative OGT activity in absence of an inhibitor (taken as 100). The data suggests a number of the compounds were able to inhibit hOGT activity. The most effective inhibitors here were found to be bear analogues of the α -A crystallin derived sequence rather than VTPVSTA. Indeed, conjugate **31** bearing the VTPVSTA sequence did not display significant inhibitory effects under these conditions. The most pronounced inhibitory effects were displayed by **23** and **26**, inhibiting OGT activity by ~40%. Conjugate **33**, derived from modifying GlcNAc, seemed to display some activity, however the results were inconclusive. GlcNAc-based bisubstrate inhibitors have not yet been investigated for use against OGT.

In pursuit of a better understanding of the interactions of bisubstrate



Scheme 3. Synthesis of a panel of novel bisubstrate analogue inhibitors (**22–33**). Reagents and conditions: (a) Fmoc-SPPS 1. Fmoc removal: 10% v/v piperidine/DMF, 2. Amino acid coupling: Fmoc-Xaa-OH (4 equiv.), PyBOP (4 equiv.), NMM (8 equiv.), DMF, 3. Capping: 10% v/v Ac₂O/pyridine; (b) 1. Fmoc removal: 10% v/v piperidine/DMF, 2. Donor analogue coupling: one of **6** or **10** (1–2 equiv.), HATU (4 equiv.), NMM (8 equiv.), DMF, 3. Resin cleavage: 90:5:5 CF₃CO₂H/TIS/H₂O, Et₂O wash, 4. Purification by RP-HPLC.

analogue inhibitors with hOGT protein, molecular docking was performed using a representative molecular scaffold. The uridine-squaramide-*N*-pentane **34** fragment molecule (Fig. 4A) was first docked into the active site of hOGT (PDB 4GZ5) [22] (Fig. 4B). The docked pose of this structure exhibited good overlap with the natural ligand UDP-GlcNAc. Notably, the uracil ring was found to participate in similar stabilising hydrogen-bonding interaction with the backbone nitrogen of Ala-896 to that of the substrate. One of the amide oxygens on the squaramide moiety was engaged in polar interactions with the zeta nitrogen (N ζ) of Lys-842, similar to the ionic interactions between the beta phosphate of UDP-GlcNAc and N ζ of Lys-842. On the other hand, the other squaramide oxygen is accepting a hydrogen bond from the backbone nitrogen of Gln-839, while the alpha phosphate of substrate accepts a hydrogen bond from the epsilon nitrogen (N ϵ) of Gln-839. These observations suggest that the bioisosteric squaramide indeed mimics pyrophosphate interactions with hOGT. Besides, the pentane linker is suggested to coil into part of the space occupied by the GlcNAc unit of

the native substrate.

We then attempted to dock bisubstrate analogue **22**. Unlike **34**, this compound could not be docked into the same active site as UDP-GlcNAc. Instead, its docked pose lies on top of the UDP-GlcNAc site (Fig. 4C), in a similar position to a 14-meric peptide substrate previously studied [18] although their structural overlap is relatively poor. We reasoned, the lack of potency of these bisubstrate analogues is due to the peptide binding in a different location that resulted into pulling the squaramide away from its ideal UDP-GlcNAc binding site. Despite that these analogues may not occupy and take advantage of the UDP-GlcNAc binding site, they could still interrupt interactions between hOGT and the acceptor protein/peptide.

The results of the docking simulations suggest that, although the squaramide is a capable pyrophosphate isostere, its inclusion does not necessarily qualify bisubstrate structures as potent inhibitors. The fact that **22** could not be docked into the desired binding site suggests that the bisubstrate analogues may not satisfy the structural criteria of an

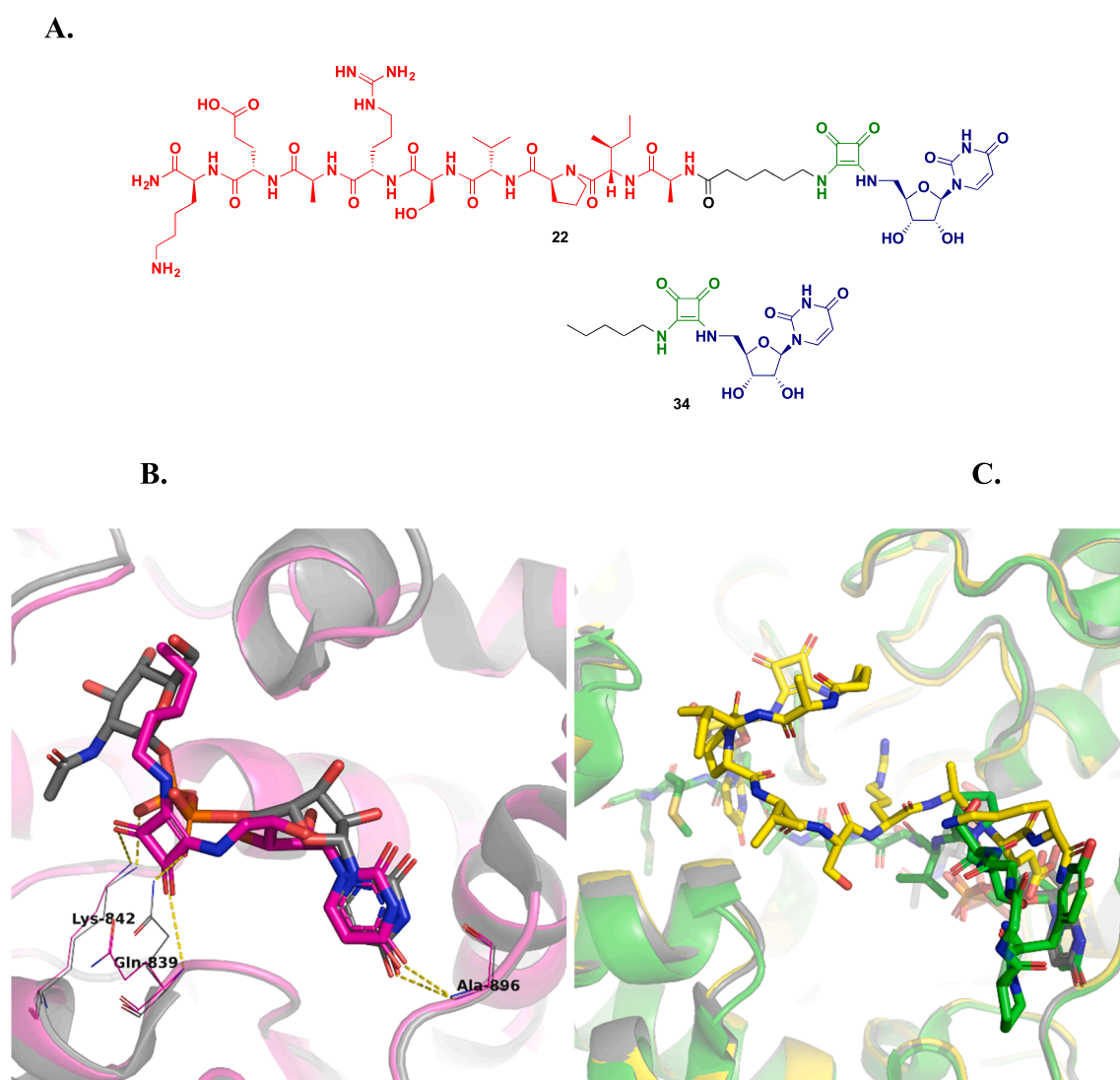


Fig. 4. (A) Chemical structures of **22** and uridine-squaramide-*N*-pentane **34**. (B) Superimposition of the docked pose of a UDP-linker structure **34** (magenta carbons and cartoons) and a hOGT:UDP-GlcNAc structure from PDB 4GZ5 (grey carbons and cartoons). Protein structures are displayed by cartoons while ligand structures are shown in thick sticks. Some interacting residues also labelled and shown by thin sticks. Yellow dashed lines indicate polar/ionic interactions. Other atoms are coloured in blue (nitrogen), red (oxygen), and orange (phosphorus). (C) Superimposition of the docked pose of bisubstrate analogue **22** (yellow carbons and cartoons), a hOGT:UDP-GlcNAc structure from PDB 4GZ5 (grey carbons and cartoons), and a hOGT:UDP-GlcNAc:peptide structure from PDB 3PE4 (green carbons and cartoons). Protein structures are displayed by cartoons while ligand/peptide structures are shown in thick sticks. Other atoms are coloured in blue (nitrogen), red (oxygen), orange (phosphorus), and dark yellow (sulphur). (For interpretation of the references to colour in this figure legend, the reader is referred to the web version of this article.)

effective inhibitor. Indeed, this is the first study to explore the effectiveness of inhibitors tethered *via* the acceptor substrate analogues *N*-termini. Other reported bisubstrate conjugates to date have been tethered to central residues of their acceptor analogue sequences *via* short aliphatic linkers [30]. It is possible that the potencies of the conjugates were impacted by their inability to adopt conformations that aligned the donor and/or acceptor moieties with those in the Michaelis complex. Hence, the trends in inhibition achieved upon modulating the acceptor sequences herein may not be reflective of the effects of modulating the acceptor sequence adopting the native conformation within the active site. Docking with **22** suggests the inhibition could result from alternative binding modes, though supplemental evidence supporting this was not pursued. Nevertheless, it was found that the conjugates bearing α -A crystallin derived sequences closer to the native sequence were more active than those heavily modified. Interestingly, the conjugate with the sequon-derived VTPVSTA acceptor analogue (**31**) was not as effective at inhibiting hOGT activity.

4. Concluding remarks

OGT inhibitors are required to better understand OGT functions. The design of OGT inhibitors is particularly challenging due to the enzyme's large, hydrophilic, and promiscuous active site. Recently, the Walker group has further explored the basic scaffold and reported the highly active OGT inhibitor OSMI-4 (EC₅₀ ~ 3 μ M in cell) although still it needs to be evaluated for its safe application *in-vitro* and *in-vivo* [54]. In this study, we report the first examples of functional hOGT bisubstrate inhibitors that feature an established bioisosteric replacement for the problematic pyrophosphate moiety as well as *in silico* support for this replacement's applicability in design of novel OGT inhibitors. The conjugates featured herein also represent the first examples of *N*-terminally tethered hOGT bisubstrate inhibitors possessing reasonable activity against recombinant hOGT activity. We expect that optimization of the structure of these novel hOGT bisubstrate inhibitors will lead to improved inhibition.

Declaration of Competing Interest

The authors declare that they have no known competing financial interests or personal relationships that could have appeared to influence the work reported in this paper.

Acknowledgements

Financial support to SR from an Australian Research Council – Discovery Early Career Researcher Award (DE140101632) is gratefully acknowledged. Authors would like to thank Prof David J. Vocadlo and Dr Matthew Alteen (Simon Fraser University, Canada) for performing enzyme inhibition assay and helpful discussion. SR expresses his sincere gratitude to Prof Richard J. Payne and Prof Kate Jolliffe (The University of Sydney) for their support. PR is supported by Griffith University Postgraduate Research Scholarship (GUPRS). Authors thank Vivek Makwana for assistance with creating graphics.

Appendix A. Supplementary data

Supplementary data to this article can be found online at <https://doi.org/10.1016/j.bioorg.2021.104738>.

References

- [1] C.R. Torres, G.W. Hart, Topography and polypeptide distribution of terminal *N*-acetylglucosamine residues on the surfaces of intact lymphocytes. Evidence for *O*-linked GlcNAc, *J. Biol. Chem.* 259 (1984) 3308–3317.
- [2] G.W. Hart, M.P. Housley, C. Slawson, Cycling of *O*-linked β -*N*-acetylglucosamine on nucleocytoplasmic proteins, *Nature* 446 (2007) 1017–1022.

- [3] L. Wells, K. Vosseller, G.W. Hart, Glycosylation of nucleocytoplasmic proteins: signal transduction and *O*-GlcNAc, *Science* 291 (2001) 2376–2378.
- [4] D.C. Love, J.A. Hanover, The hexosamine signaling pathway: deciphering the “*O*-GlcNAc code”, *Sci. STKE* (2005) re13.
- [5] N.E. Zachara, G.W. Hart, Cell signaling, the essential role of *O*-GlcNAc!, *Biochim. Biophys. Acta* 1761 (2006) 599–617.
- [6] J. Ma, G.W. Hart, Protein *O*-GlcNAcylation in diabetes and diabetic complications, *Expert Rev. Proteomic.* 10 (2013) 365–380.
- [7] X. Yang, P.P. Ongusaha, P.D. Miles, J.C. Havstad, F. Zhang, W.V. So, J.E. Kudlow, R.H. Michell, J.M. Olefsky, S.J. Field, R.M. Evans, Phosphoinositide signalling links *O*-GlcNAc transferase to insulin resistance, *Nature* 451 (2008) 964–969.
- [8] S.A. Caldwell, S.R. Jackson, K.S. Shahriari, T.P. Lynch, G. Sethi, S. Walker, K. Vosseller, M.J. Reginato, Nutrient sensor *O*-GlcNAc transferase regulates breast cancer tumorigenesis through targeting of the oncogenic transcription factor FoxM1, *Oncogene* 29 (2010) 2831–2842.
- [9] T.P. Lynch, C.M. Ferrer, S.R. Jackson, K.S. Shahriari, K. Vosseller, M.J. Reginato, Critical role of *O*-linked beta-*N*-acetylglucosamine transferase in prostate cancer invasion, angiogenesis, and metastasis, *J. Biol. Chem.* 287 (2012) 11070–11081.
- [10] V. Makwana, P. Ryan, B. Patel, S.-A. Dukie, S. Rudrawar, Essential role of *O*-GlcNAcylation in stabilization of oncogenic factors, *BBA - Gen. Subjects* 2019 (1863) 1302–1317.
- [11] S.A. Marsh, H.E. Collins, J.C. Chatham, Protein *O*-GlcNAcylation and cardiovascular (patho)physiology, *J. Biol. Chem.* 289 (2014) 34449–34456.
- [12] S.A. Yuzwa, X. Shan, M.S. Macauley, T. Clark, Y. Skorobogatko, K. Vosseller, D. J. Vocadlo, Increasing *O*-GlcNAc slows neurodegeneration and stabilizes tau against aggregation, *Nat. Chem. Biol.* 8 (2012) 393–399.
- [13] B.D. Lazarus, D.C. Love, J.A. Hanover, *O*-GlcNAc cycling: implications for neurodegenerative disorders, *Int. J. Biochem. Cell Biol.* 41 (2009) 2134–2146.
- [14] P. Ryan, M. Xu, A.K. Davey, J.J. Danon, G.D. Mellick, M. Kassiou, S. Rudrawar, *O*-GlcNAc modification protects against protein misfolding and aggregation in neurodegenerative disease, *ACS Chem. Neurosci.* 10 (2019) 2209–2221.
- [15] Y. Gao, L. Wells, F.I. Comer, G.J. Parker, G.W. Hart, Dynamic *O*-glycosylation of nuclear and cytosolic proteins: cloning and characterization of a neutral, cytosolic β -*N*-acetylglucosaminidase from human brain, *J. Biol. Chem.* 276 (2001) 9838–9845.
- [16] S.A. Yuzwa, X. Shan, B.A. Jones, G. Zhao, M.L. Woodward, X. Li, Y. Zhu, E. J. McEachern, M.A. Silverman, N.V. Watson, C.X. Gong, D.J. Vocadlo, Pharmacological inhibition of *O*-GlcNAc transferase (OGA) prevents cognitive decline and amyloid plaque formation in bigenic tau/APP mutant mice, *Mol. Neurodegener.* 9 (2014) 42.
- [17] E.J. Kim, M.R. Bond, D.C. Love, J.A. Hanover, Chemical tools to explore nutrient-driven *O*-GlcNAc cycling, *Crit. Rev. Biochem. Mol. Biol.* 49 (2014) 327–342.
- [18] M.B. Lazarus, Y. Nam, J. Jiang, P. Sliz, S. Walker, Structure of human *O*-GlcNAc transferase and its complex with a peptide substrate, *Nature* 469 (2011) 564–567.
- [19] R.J. Konrad, F. Zhang, J.E. Hale, M.D. Knierman, G.W. Becker, J.E. Kudlow, Alloxan is an inhibitor of the enzyme *O*-linked *N*-acetylglucosamine transferase, *Biochem. Biophys. Res. Commun.* 293 (2002) 207–212.
- [20] H.C. Dorfmüller, V.S. Borodkin, D.E. Blair, S. Pathak, I. Navratilova, D.M. van Aalten, Substrate and product analogues as human *O*-GlcNAc transferase inhibitors, *Amino Acids* 40 (2011) 781–792.
- [21] T.M. Gloster, W.F. Zandberg, J.E. Heinonen, D.L. Shen, L. Deng, D.J. Vocadlo, Hijacking a biosynthetic pathway yields a glycosyltransferase inhibitor within cells, *Nat. Chem. Biol.* 7 (2011) 174–181.
- [22] M.B. Lazarus, J. Jiang, T.M. Gloster, W.F. Zandberg, G.E. Whitworth, D.J. Vocadlo, S. Walker, Structural snapshots of the reaction coordinate for *O*-GlcNAc transferase, *Nat. Chem. Biol.* 8 (2012) 966–968.
- [23] M. Schimpl, X. Zheng, V.S. Borodkin, D.E. Blair, A.T. Ferenbach, A. W. Schüttelkopf, I. Navratilova, T. Aristotelous, O. Albarbarawi, D.A. Robinson, M. A. Macnaughtan, D.M.F. van Alten, *O*-GlcNAc transferase invokes nucleotide sugar pyrophosphate participation in catalysis, *Nat. Chem. Biol.* 12 (2012) 969–974.
- [24] I. Tvaroška, S. Kozmon, M. Wimmerová, J. Koča, Substrate-assisted catalytic mechanism of *O*-GlcNAc transferase discovered by quantum mechanics/molecular mechanics investigation, *J. Am. Chem. Soc.* 134 (2012) 15563–15571.
- [25] M. Izumi, H. Yuasa, H. Hashimoto, Bisubstrate analogues as glycosyltransferase inhibitors, *Curr. Top. Med. Chem.* 9 (2009) 87–105.
- [26] Vladimir S. Borodkin, M. Schimpl, M. Gundogdu, K. Rafie, Helge C. Dorfmüller, David A. Robinson, Daan M.F. van Aalten, Bisubstrate UDP-peptide conjugates as human *O*-GlcNAc transferase inhibitors, *Biochem. J.* 457 (2014) 497–502.
- [27] H. Zhang, T. Tomasić, J. Shi, M. Weiss, R. Ruijtenbeek, M. Anderlüh, R.J. Pieters, Inhibition of *O*-GlcNAc transferase (OGT) by peptidic hybrids, *MedChemComm* 9 (2018) 883–887.
- [28] D. Derossi, A.H. Joliot, G. Chassaing, A. Prochiantz, The third helix of the Antennapedia homeodomain translocates through biological membranes, *J. Biol. Chem.* 269 (1994) 10444–10450.
- [29] E. Vives, P. Brodin, B. Lebleu, A truncated HIV-1 Tat protein basic domain rapidly translocates through the plasma membrane and accumulates in the cell nucleus, *J. Biol. Chem.* 272 (1997) 16010–16017.
- [30] K. Rafie, A. Gorelik, R. Trapannone, V.S. Borodkin, D.M.F. van Aalten, Thio-linked UDP-peptide conjugates as *O*-GlcNAc transferase inhibitors, *Bioconjug. Chem.* 29 (2018) 1834–1840.
- [31] S. Wang, D.L. Shen, D. Lafont, A.-S. Vercoutter-Edouart, M. Mortuaire, Y. Shi, O. Maniti, A. Girard-Egrot, T. Lefebvre, B.M. Pinto, D. Vocadlo, S. Vidal, Design of glycosyltransferase inhibitors targeting human *O*-GlcNAc transferase (OGT), *MedChemCommun* 5 (2014) 1172–1178.

- [32] J. Jiang, M.B. Lazarus, L. Pasquina, P. Sliz, S. Walker, A neutral diphosphate mimic crosslinks the active site of human O-GlcNAc transferase, *Nat. Chem. Biol.* 8 (2011) 72–77.
- [33] B.J. Gross, B.C. Kraybill, S. Walker, Discovery of O-GlcNAc transferase inhibitors, *J. Am. Chem. Soc.* 127 (2005) 14588–14589.
- [34] T.S. Elliott, A. Slowey, Y. Ye, S.J. Conway, The use of phosphate bioisosteres in medicinal chemistry and chemical biology, *MedChemCommun* 3 (2012) 735–751.
- [35] D. Quiñero, A. Frontera, P. Ballester, P.M. Deyà, A theoretical study of aromaticity in squaramide and oxocarbons, *Tetrahedron Lett.* 41 (2000) 2001–2005.
- [36] S. Tomàs, R. Prohens, M. Vega, M.C. Rotger, P.M. Deyà, P. Ballester, A. Costa, Squaramido-based receptors: design, synthesis, and application to the recognition of tetraalkylammonium compounds, *J. Org. Chem.* 61 (1996) 9394–9401.
- [37] K. Seo, T. Miyashita, K. Sato, M. Sekine, Synthesis and properties of new nucleotide analogues possessing squaramide moieties as new phosphate isosteres, *Eur. J. Org. Chem.* 2005 (2005) 5163–5170.
- [38] S. Niewiadomski, Z. Beebejaun, H. Denton, T.K. Smith, R.J. Morris, G.K. Wagner, Rationally designed squaryldiamides - a novel class of sugar-nucleotide mimics? *Org. Biomol. Chem.* 8 (2010) 3488–3499.
- [39] K.A. Winans, C.R. Bertozzi, An inhibitor of the human UDP-GlcNAc 4-epimerase identified from a uridine-based library: a strategy to inhibit O-linked glycosylation, *Chem. Biol.* 9 (2002) 113–129.
- [40] A. Babić, S. Gobec, C. Gravier-Pelletier, Y. Le Merrer, S. Pečar, Synthesis of 1-C-linked diphosphate analogues of UDP-N-Ac-glucosamine and UDP-N-Ac-muramic acid, *Tetrahedron* 64 (2008) 9093–9100.
- [41] N. Gavande, H.L. Kim, M.R. Doddareddy, G.A. Johnston, M. Chebib, J. R. Hanrahan, Design, synthesis, and pharmacological evaluation of fluorescent and biotinylated antagonists of rho1 GABAC receptors, *ACS Med. Chem. Lett.* 4 (2013) 402–407.
- [42] X. Cai, T. Whitfield, M.S. Hixon, Y. Grant, G.F. Koob, K.D. Janda, Probing active cocaine vaccination performance through catalytic and noncatalytic hapten design, *J. Med. Chem.* 56 (2013) 3701–3709.
- [43] C.H. Lee, H.J. Yun, M.R. Jung, J.G. Lee, S.H. Kim, J.H. Kim, Preparation and characterization of squaraine dyes containing mono- and bis-anchoring groups as the light absorber in dye sensitized solar cells, *Electrochim. Acta* 138 (2014) 148–154.
- [44] D. Yan, J. Naughton, M. Clyne, P.V. Murphy, Synthesis of bivalent glycoclusters containing GlcNAc as hexasaccharide mimetics. Bactericidal activity against *Helicobacter pylori*, *Carbohydr. Res.* 360 (2012) 1–7.
- [45] P. Ryan, A.H.W. Koh, A.E. Lohning, S. Rudrawar, Solid-phase O-glycosylation with a glucosamine derivative for the synthesis of a glycopeptide, *Aust. J. Chem.* 70 (2017) 1151–1157.
- [46] D.L. Shen, T.M. Gloster, S.A. Yuzwa, D.J. Vocadlo, Insight into O-linked N-acetylglucosamine (O-GlcNAc) processing and dynamic through kinetic analysis of O-GlcNAc transferase and O-GlcNAcase activity on protein substrates, *J. Biol. Chem.* 287 (2012) 15395–15408.
- [47] W. Sherman, T. Day, M.P. Jacobson, R.A. Friesner, R. Farid, Novel procedure for modeling ligand/receptor induced fit effects, *J. Med. Chem.* 49 (2006) 534–553.
- [48] R.A. Friesner, J.L. Banks, R.B. Murphy, T.A. Halgren, J.J. Klicic, D.T. Mainz, M. P. Repasky, E.H. Knoll, M. Shelley, J.K. Perry, D.E. Shaw, P. Francis, P.S. Shenkin, Glide: a new approach for rapid, accurate docking and scoring. 1. Method and assessment of docking accuracy, *J. Med. Chem.* 47 (2004) 1739–1749.
- [49] T.A. Halgren, R.B. Murphy, R.A. Friesner, H.S. Beard, L.L. Frye, W.T. Pollard, J. L. Banks, Glide: a new approach for rapid, accurate docking and scoring. 2. Enrichment factors in database screening, *J. Med. Chem.* 47 (2004) 1750–1759.
- [50] M.P. Jacobson, R.A. Friesner, Z. Xiang, B. Honig, On the role of the crystal environment in determining protein side-chain conformations, *J. Mol. Biol.* 320 (2002) 597–608.
- [51] T.M. Leavy, C.R. Bertozzi, A high-throughput assay for O-GlcNAc transferase detects primary sequence preferences in peptide substrates, *Bioorg. Med. Chem. Lett.* 17 (2007) 3851–3854.
- [52] R.M. Kini, Proline brackets and identification of potential functional sites in proteins: toxins to therapeutics, *Toxicon* 36 (1998) 1659–1670.
- [53] S. Pathak, J. Alonso, M. Schimpl, K. Rafie, D.E. Blair, V.S. Borodkin, O. Albarbarawi, D.M.F. van Aalten, The active site of O-GlcNAc transferase imposes constraints on substrate sequence, *Nat. Struct. Mol. Biol.* 22 (2015) 744–750.
- [54] S.E.S. Martin, Z.-W. Tan, H.M. Itkonen, D.Y. Duveau, J.A. Paulo, J. Janetzko, P. L. Boutz, L. Törk, F.A. Moss, C.J. Thomas, S.P. Gygi, M.B. Lazarus, S. Walker, Structure-based evolution of low nanomolar O-GlcNAc transferase inhibitors, *J. Am. Chem. Soc.* 140 (2018) 13542–13545.